UDC 004.8:621.39 **doi: 10.32620/aktt.2025.6.05**

Vladimir LUKIN[1], Volodymyr REBROV[1], Andrii PAVLIUK[2]

[1] *National Aerospace University «Kharkiv Aviation Institute», Kharkiv, Ukraine*
[2] *National Technical University of Ukraine «Igor Sikorsky Kyiv Polytechnic Institute», Kyiv, Ukraine*

LOSSY COMPRESSION OF MULTILOOK SAR IMAGES IN THE OPTIMAL OPERATION POINT NEIGHBORHOOD BY BPG-CODER

*The **subject matter** of the article is the process of lossy compression of multilook Synthetic Aperture Radar (SAR) images corrupted by multiplicative, spatially correlated speckle noise, with a focus on operation in the neighborhood of the potential Optimal Operation Point (OOP). The **goal** of the article is to analyze the existence and properties of the OOP for SAR image compression using the Better Portable Graphics (BPG) coder, and to develop a practical method for achieving compression near this point. The **tasks** to be solved are: to verify the existence of the OOP for simulated Sentinel-1-like SAR images according to both traditional peak signal-to-noise ratio (PSNR) and visual quality (PSNR-HVS-M) metrics; to investigate the relationship between the compression control parameter (Q) and the resulting image quality and compression ratio (CR); and to propose and describe a practical iterative procedure for determining the Q parameter value corresponding to the OOP without requiring access to the noise-free reference image. The **methods** used are: simulation of SAR images with speckle relative variance equal to 0.05 using noise-free Sentinel-2 data as a reference; lossy compression using the BPG coder with parameter Q varying from 1 to 51; quantitative assessment using PSNR and PSNR-HVS-M metrics; calculation of compression ratio; analysis of rate-distortion curves between different image pairs; statistical estimation of equivalent noise variance for input PSNR prediction. The following **results** were obtained: It has been demonstrated that an OOP exists for the BPG coder when compressing multilook SAR images, confirmed by both PSNR and PSNR-HVS-M metrics. The OOP provides PSNR and PSNR-HVS-M values several dB higher compared to the uncompressed noisy image while achieving very high compression ratios (CR > 180). The OOP was found at high Q values (Q=48-49), where the coder aggressively suppresses noise but also introduces content distortions. A key practical result is the proposed method for determining Q at the OOP. **Conclusions.** The scientific novelty of the obtained results is as follows: For the first time, the existence of the OOP has been comprehensively demonstrated for the BPG coder applied to multilook SAR images with realistic speckle properties, considering not only the standard PSNR but also the visual quality metric PSNR-HVS-M, although the OOP is less pronounced for the latter; a method for practical OOP approximation has been developed, which operates without the need for the original noise-free (true) image, relying instead on an estimation of the speckle noise power from the available noisy data, making it applicable in real-world SAR image processing and transmission scenarios.*

Keywords: *synthetic aperture radar, lossy compression, speckled image, optimal operation point.*

1. Introduction

1.1. Motivation

Remote sensing (RS) systems have become a tool for solving various tasks in ecological monitoring [1], defense [2], oceanography [3], etc. For aforementioned and other applications, synthetic aperture radars (SARs) are used due to reliable operation in all-weather conditions and high spatial resolution [3, 4]. Meanwhile, average size of SAR images has an obvious tendency to increase. Then, to transfer SAR images from on-board to on-land and, later, to disseminate them, compression is needed [6,7]. Lossless compression is applied rarely since the provided compression ratio (CR) is usually only slightly larger than unity [8] because of speckle present in SAR images. Then, lossy compression is employed that has been of high attention both 30 years ago[5] and now [6,7].

Speckle is a noise-like phenomenon of multiplicative nature, which happens for any type of imaging carried out by coherent systems [9]. Speckle and its properties have to be taken into account practically in any kind of SAR image processing such as including edge and target detection [10], denoising [11], lossy compression [12, 13], and so on. Note that lossy compression noisy images is characterized by several specific effects [14]. This is, first, noise filtering effect, and, second, possible existence of optimal operation point (OOP) where a compressed image is the closest (most similar) to the corresponding noise-free

ISSN 1814-4225 (print)
ISSN 2663-2012 (online)

image [14]. Possible existence of OOP was demonstrated for SAR images [13, 15] compressed by several known coders. Compression is OOP is attractive since two benefits are achieved simultaneously – quite high quality and quite large CR.

Recently, new efficient coders such as better portable graphics (BPG) [16], AVIF [17], HEIF [18], and some others have been proposed. It has been shown [14] that they are able to perform well enough for images corrupted by additive white Gaussian noise. These (and other) coders have been also tested for visually lossless [13, 19] compression of SAR images in [20] using several modern visual quality metrics [21] and thresholds of distortion invisibility for them [22, 23]. However, possibility of attaining OOP for them in lossy compression of SAR images has not been studied. Thus, we concentrate on the BPG coder and its performance in the considered application below.

1.2. State-of-the-art

In lossy compression of noisy images in general and SAR images in particular, the main goal is to provide acceptable quality of compressed images simultaneously with rather large CR. Because of this, there are several possible strategies [6, 13] that can be realized depending on priority of requirements and imposed restrictions. One idea is to perform the so-called visually lossless compression [20] where post-filtering can be carried on-land after decompression. A positive feature of this strategy is that a rather high quality of decompressed and then post-filtered images can be provided due to application of filters adapted to speckle properties. However, the drawback is that the provided CR is quite low – about 3 for 8-bit representation of original SAR images and slightly more if more bits are employed for SAR image representation [20].

Keeping aforementioned drawback in mind, other strategies are possible. One of them presumes SAR image lossy compression in OOP or its neighborhood [6, 13]. Possible existence of OOP in lossy compression of noisy images has been shown for different types of noise [14, 15] and for different lossy compression techniques including old standards such as JPEG [24] and JPEG2000 [6] as well as modern coders [14]. There are three main problems concerning compression in OOP. First, OOP exists not always. For a given noisy image, it might exist for one coder and not exist for another coder where the general tendency is the higher probability of OOP existence for more modern coders [14]. Similarly, it might exist according to one metric and not exist for another metric where the general tendency is the higher probability for PSNR compared to visual quality metrics. Finally, for a given noise intensity, OOP might exist for one image and not exist for another image where OOP exists more often for simpler structure images. Then, trying to compress a noisy image in OOP, one should be sure that OOP for this image exists. Prediction of OOP existence is a particular task not considered in this paper.

Second, it is necessary to know how to set a parameter that controls compression (PCC) for a given coder to reach OOP. Here it is necessary to mention that different parameters are used in different coders as PCC. JPEG, AVIF, and HEIF employ quality factor (QF) where a larger QF corresponds to less distortions introduced into the compressed image and smaller CR. JPEG2000 uses bits per pixel (BPP) as PCC where a larger BPP relates to smaller distortions and smaller CR. The BPG coder employs Q (integer from 1 to 51) where a larger Q produces larger distortions and larger CR. In this paper, we consider just the BPG coder.

Third, speckle noise in SAR images is usually spatially correlated [25]. There is a very little number of papers devoted to lossy compression of images corrupted by spatially correlated noise [26]. It is shown there that OOP is possible but it is less obvious than for the same true image corrupted by white noise with the same variance. Besides, PCC in OOP for these two cases can be slightly different.

Then, we deal with a quite complex case of lossy compression of images corrupted by multiplicative spatially correlated noise. To start from a slightly simpler case, we consider multilook SAR images for which speckle distribution is more close to Gaussian than for single-look images.

1.3. Objectives and the approach

Our goal is to analyze does OOP exist in lossy compression of SAR images with realistic properties of speckle by the BPG coder and, if OOP is possible, what are the PCC properties for OOP. We focus on images simulating Sentinel-1 [27] SAR data that has been widely exploited in recent years for various applications [28, 29]. In other words, our simulated images have the same statistical and spatial correlation properties as multilook images produces by Sentinel-1 in dual-polarization mode. In addition to standard PSNR, we consider the PSNR-HVS-M visual quality metric (https://ponomarenko.info/psnrhvsm.htm), which is also expressed in dB and incorporates important peculiarities of human vision system (HVS).

The paper structure is as follows. Section 2 deals with the image/noise model and traditional rate/distortion curves. Rate/distortion curves calculated between true an noisy compressed images are analyzed in Section 3 with showing the OOP existence according to two metrics. Compression examples demonstrating speckle suppression and discussion are given in Section 4. Finally, the Conclusions follow.

2. Materials and methods of research

One additional problem in analysis of SAR image lossy compression is the absence of commonly accepted true images as well as methods and tools for speckle simulation [30, 31]. Because of this, noise-free images are often taken from practically noise-free components of multispectral Sentinel-2 data [32].

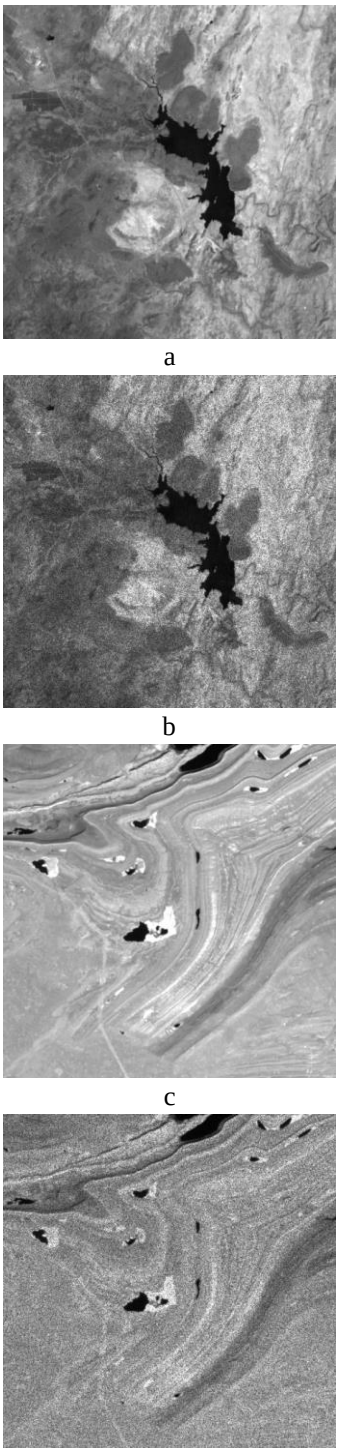

a

b

c

d

Fig. 1. Noise-free test image #1 (a), its noisy version (b), noise-free test image #2 (c) and its noisy version (d)

After this, speckle noise with statistical and spatial correlation properties determined for speckle in multi-look Sentinel-1 SAR images is artificially added. Speckle relative variance is approximately equal to 0.05.

Fig. 1 presents two typical noise-free remote sensing images further called Test image #1 (Fig. 1,a) and Test image #2 (Fig. 1,c). Noisy images for these test images are represented in Figures 1,b and 1,d. It is easy to notice that speckle is observed in homogeneous image regions (except very dark regions that correspond to smaller mean intensity and, respectively, to less intensive fluctuations according to the multiplicative noise model). Due to intensive speckle, low contrast small-sized and prolonged objects as well low contrast textures are severely deteriorated and/or masked. This explains why it is worth removing speckle by filtering or suppressing it at lossy compression stage.

Meanwhile, speckle reduction should be careful to preserve edges, fine details, and textural features. These requirements of efficient speckle suppression and simultaneous preservation of information features are contradictory and an appropriate trade-off should be found in coder selection and its parameters setting.

Below, we consider SAR image representation as 8-bit (integer-valued) 2D data arrays. In general, SAR images are often represented as arrays with a larger number of bits. However, our solution to use 8-bit representation deals with the following reasons.

First, not all existing metrics including visual quality ones can be calculated for data with arbitrary number of bits. Second, preliminary normalization of images to the range 0-255 and back introduce significantly less distortions than distortions due to lossy compression, especially in OOP neighborhood. Thus, we further ignore distortions due to direct and inverse normalizations.

The BPG-coder realization intended to compress single-channel (grayscale) images freely available at https://bellard.org/bpg/ has been applied. This coder, similarly to JPEG, is based on discrete cosine transform (DCT) but it is able to adapt to image content. Due to this, the BPG coder usually outperforms JPEG and the benefit is the most significant for simple structure images and images of various content. In opposite to JPEG, the BPG-coder performance is controlled by aforementioned parameter Q where the level of introduced distortions varies in wide limits and the worst image quality is produced for Q approaching 51.

In theory and practice of lossy compression applied to noise-free images, metrics of quality are mainly determined between images before and after compression. In this sense, let us briefly consider dependences of $PSNR_{nc}$ determined between noisy images and their compressed counterparts. They are presented in Fig. 2.

ISSN 1814-4225 (print)
ISSN 2663-2012 (online)

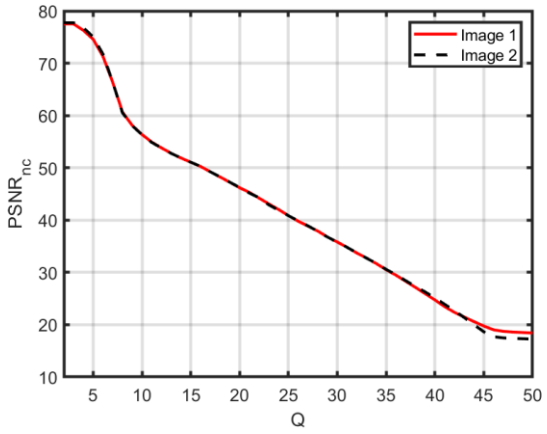

Fig. 2. Dependences of $PSNR_{nc}(Q)$ for test images

In general, these dependences are typical for the BPG coder [32] where a metric characterizing distortions due to lossy compression makes worse (indicates more distortions) if Q increases. The dependences in Fig. 2 have three main intervals. For $Q<10$, distortions are negligible ($PSNR_{nc}>56$ dB) and the curve behaves in nonlinear manner. Then, for $10\le Q\le 45$, $PSNR_{nc}$ decreases practically linearly where $PSNR_{nc}\approx 65-Q$ for both test images. Finally, for $Q>45$, $PSNR_{nc}$ continues decreasing but the decreasing speed becomes smaller and the curves "diverge". Note that, for $Q>45$, the introduced distortions are very large and, if 8-bit representation is used, mean square error of these distortions is about 1000.

One more type of curves can be of particular interest. Fig. 3 shows dependences of CR on Q. They behave similarly for the considered test images. If $Q\le 30$, the introduced distortions are not visible but CR values are smaller than 3 [20]. Just this obstacle explains some limitations on visually lossless compression since a desired CR can be considerably larger. Till Q=40, CR increases but continues to be quite small. However, starting from $Q\approx 43$, CR begins to increase radically reaching approximately 100 for $Q\approx 47$ and approximately 250 for Q=50, i.e. the interval of $43\le Q\le 51$ should be of particular interest for lossy compression.

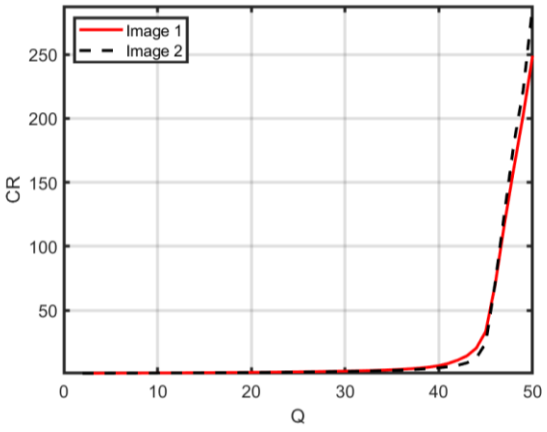

Fig. 3. Dependences of CR on Q for both test images

3. OOP Analysis for the Considered Images

3.1. Obtained rate/distortion curves

Consider rate/distortion curves (RDCs) obtained for compressed noisy and test images (subindex tc relates to such curves). Dependences $PSNR_{tc}(Q)$ are presented in Fig. 4. They have behavior that has distinctive difference compared to $PSNR_{nc}(Q)$ (see Fig. 1). First of all, both RDCs $PSNR_{tc}(Q)$ remain practically constant for $Q<35$ and this confirms that compressed images for this interval look practically the same. Then, for $35\le Q\le 47$, $PSNR_{tc}(Q)$ increases if Q becomes larger. This improvement of quality is mainly associated with better speckle suppression, whilst distortions introduced into image content also increase (negative effect) but not so quickly as noise removal (positive effect). Finally, OOP is observed for Q=49 for the test image #1 and for Q=48 for the test image #2. After this, $PSNR_{tc}(Q)$ starts to decrease.

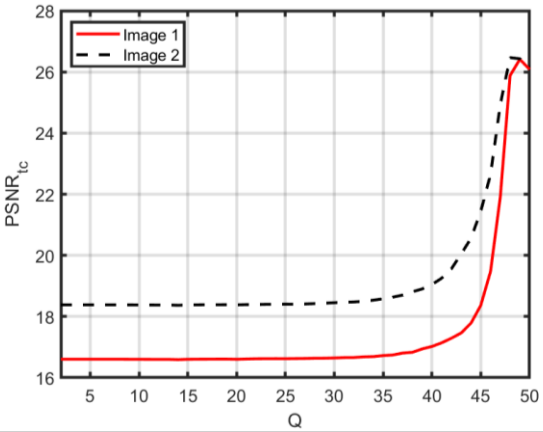

Fig. 4. Dependences $PSNR_{tc}(Q)$ for the test images

Thus, we can state that OOPs are observed for both test images and these OOPs are "obvious" in the sense that $PSNR_{tc}(Q=Q_{OOP})$ is significantly (by about 8-9 dB) larger than $PSNR_{tc}(Q=1)\approx PSNR_n$ where $PSNR_n$ is PSNR of noisy (uncompressed) image with respect to the true image.

The results obtained for lossy compression of noisy images by different coders [14] show that OOP might take place not only for PSNR metric but for other metrics, including visual quality ones, as well. So, let us check whether or not this happens for lossy compression of SAR images. Fig. 5 shows RDCs PSNR-HVS-$M_{tc}(Q)$ for the considered test images.

As seen, these RDCs have behavior very similar to RDCs $PSNR_{tc}(Q)$ in Fig. 4. There are OOPs that are observed for the same values of Q_{OOP} as in in Fig. 4. Thus, we can state that OOPs for both metrics, $PSNR_{tc}$ and PSNR-HVS-M_{tc} take place for the same Q_{OOP}, and this is a positive moment. However, the OOPs for PSNR-

HVS-M_{tc} are not so obvious as for the metric $PSNR_{tc}$. Really, PSNR-HVS-$M_{tc}(Q=Q_{OOP})$ is larger by only 2-4 dB than PSNR-HVS-$M_{tc}(Q=1)$. Besides, a question remains - how to determine Q_{OOP}?

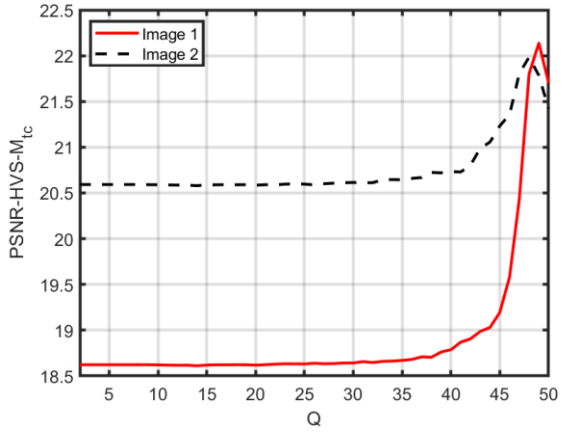

Fig. 5. Dependences PSNR-HVS-$M_{tc}(Q)$ for the considered test images

3.2. One way to determine Q_{OOP}

It has been noticed in [6] that OOP takes the place when $PSNR_{nc}(Q) \approx PSNR_n$. Note that, in practice, we cannot measure $PSNR_{tc}$ for any given Q since we do not have the true image, but we can measure $PSNR_{nc}$. The questions then are the following: 1) does the aforementioned property take the place for the considered case of SAR image compression? 2) can we measure of estimate $PSNR_n$? Let us start from answering the first question.

According to data in Fig. 4, $PSNR_n$ is approximately equal to 18.4 dB for the test image #1 it is approximately equal to 16.6 dB for the test image #2. According to the plots in Fig. 2, $PSNR_{nc}$ crosses the level 18.6 dB for Q=48 for the test image #1 and the level 16.6 dB for Q=49 for the test image #2. Thus, the aforementioned property remains.

The second question then is how to estimate $PSNR_n$, again without having the true image at hand. Recall here that

$$PSNR_n = 10 \lg\left(\frac{255^2}{\sigma_{eq}^2}\right),$$

$$\sigma_{eq}^2 = \sigma_\mu^2 \sum_{k=1}^{K} \sum_{l=1}^{L} I_{t\,kl}^2 / KL,$$

where σ_{eq}^2 is the equivalent noise variance calculated using known true image $I_{t\,kl}^2$, $k = 1, \dots, K$, $l = 1, \dots, L$, K and L denote the image size. Since the true image is not available, σ_{eq}^2 can be estimated as

$$\sigma_{eq\ est}^2 \approx \sigma_\mu^2 \sum_{k=1}^{K} \sum_{l=1}^{L} I_{n\,kl}^2 / KL,$$

where $I_{n\,kl}^2$, $k = 1, \dots, K$, $l = 1, \dots, L$ is the available noisy image, $\sigma_\mu^2 = 0.05$.

Let compare σ_{eq}^2 and $\sigma_{eq\ est}^2$. For the test image #1, σ_{eq}^2=951.1 and $\sigma_{eq\ est}^2$=819.5 For the test image #2, σ_{eq}^2=1490 and $\sigma_{eq\ est}^2$ =1182. Thus, σ_{eq}^2 and $\sigma_{eq\ est}^2$ are quite close although σ_{eq}^2 is about 20% (0.8 dB) larger. Then, having $\sigma_{eq\ est}^2$, it is possible to estimate $PSNR_n$ and adjust such Q that

$$PSNR_{nc}(Q) \approx 10 \lg(255^2 / \sigma_{eq\ est}^2) - 0.8$$

The corresponding iterative procedures exist [33]. To have a smaller number of iterations, the starting point is important. Here, recall that, according to Fig. 2, $PSNR_n = 65 - Q$, and, then, the starting $Q_{st} \approx 65 - PSNR_n$. If the estimated $PSNR_{nc}(Q_{st})$ calculated after compression and decompression is larger than the estimated $PSNR_n$, use $Q_2 = Q_{st} + 1$ and continue carrying out compression and decompression with $PSNR_{nc}$ calculation until for a given Q_i for the i-th iteration $PSNR_{nc}(Q_i) < PSNR_n$. Then, stop and use the image compressed with $Q_i - 1$ as the final result of compression. Certainly, there can be other modifications of this procedure.

4. Compression Examples and Discussion

4.1. Compression Examples

Fig. 6 presents the test images compressed in OOP (Q_{OOP}=49 for the test image #1 and Q_{OOP}=48 for the test image #2). Recall that CR in these cases are equal to 202.89 and 180.167, respectively.

Comparison of these images to the corresponding noise-free and speckled images in Figure 1 shows that, on one hand, speckle is suppressed well and high contrast objects and edges are preserved quite well. However, low contrast textures, edges, and fine details are smeared especially in regions with low mean level (e.g., left part of the image in Fig. 6,a).

4.2. Discussion

As seen, direct application of lossy compression to SAR images with speckle allows reaching OOP and gaining specific suppression of speckle, namely, speckle suppression is essential in homogeneous image regions with quite low mean intensity that look like black or dark grey areas. However, considerable detail smearing is simultaneously observed in such areas, which is

ISSN 1814-4225 (print)
ISSN 2663-2012 (online)

undesirable. One possible solution is to carry out lossy compression after appropriate variance stabilizing transform and apply inverse transform after decompression.

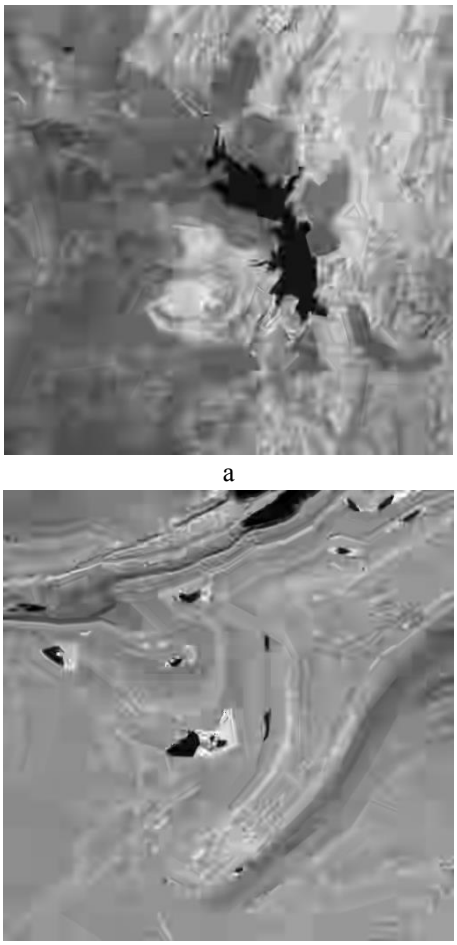

a

b

Fig. 6. Images compressed in OOP: the test image #1 (a) and test image #2 (b)

We have considered the case of $\sigma_\mu^2 = 0.05$ that corresponds to approximately 5 looks and relates to images formed by Sentinel-1 SAR. However, other SARs (e.g., TerraSAR-X) might acquire images with a smaller number of looks and, respectively, a larger σ_μ^2 , e.g., $\sigma_\mu^2 \approx 0.273$ as for single-look SAR images. Then, $PSNR_n$ can be by about 7 dB smaller than for the considered test images. Meanwhile, as it follows from data in Fig. 2, the BPG coder might be unable to provide $PSNR_n$ about 11 dB and, thus, to ensure SAR image compression in OOP. Then, other modern coders have to be tested.

4.3. Implementation example

The method we propose can be effectively implemented in onboard SAR data processing systems (e.g., Sentinel-1) to reduce data volume and mitigate the impact of speckle noise before transmission to ground stations. Furthermore, this approach can be integrated into automated remote monitoring systems, accelerating data transfer and analysis in areas such as agricultural field classification, disaster response, and environmental monitoring.

5. Conclusions

We have shown that the BPG coder applied to multilook SAR images is able to provide compression in optimal operation point determined according to PSNR and PSNR-HVS-M metrics. PSNR and PSNR-HVS-M in OOP are by several dB larger than for uncompressed images or images compressed in visually lossless manner. The attained CR are by tens of times larger than for visually lossless compression. These are the main advantages of lossy compression in OOP. The procedure for finding Q_{OOP} has been proposed.

However, some questions are not answered yet and, thus, further studies are needed. First, the use of variance stabilizing transforms before compression and after decompression has to be considered to avoid undesired smearing for areas of low intensity. Second, it is needed to design a procedure to predict OOP existence. For this purpose, more test images have to be analyzed. Third, other modern coders such as HEIF have to be studied. Finally, SAR images for small number of looks and other spatial characteristics of the speckle have to be considered.

Contributions of authors: conception – **Vladimir Lukin**; methodology – **Vladimir Lukin**; problem formulation – **Vladimir Lukin**; analysis – **Andrii Pavliuk, Volodymyr Rebrov**; model development – **Andrii Panliuk**; software – **Volodymyr Rebrov**; validation – **Vladimir Lukin**, **Volodymyr Rebrov**; analysis of results – **Andrii Pavliuk**; visualization – **Andrii Pavliuk**; writing – **Volodymyr Rebrov, Andrii Pavliuk**; revision and editing – **Vladimir Lukin**.

Conflict of interest

The authors declare that they have no conflict of interest in relation to this research, whether financial, personal, authorship, or otherwise, that could affect the research and its results presented in this paper.

Financing

The research has been funded by National Research Foundation of Ukraine (https://nrfu.org.ua/en/, accessed on 1 July 2025) within Project No. 2023. 04/0039 “Geospatial monitoring system for the war impact on the agriculture of Ukraine based on satellite data” (2024–2025).

Use of Artificial Intelligence

The authors confirm that they did not use artificial intelligence technologies when creating the current work.

All authors have read and agreed to the published version of this manuscript.

References

1. Lysenko, A. SAR Data Spatial Resolution Enhancement for Environmental Monitoring Tasks. *International Conference of Young Professionals «GeoTerrace-2023»*, 2023, vol. 2023, no. 1, pp. 1–5. DOI: 10.3997/2214-4609.2023510010.

2. Gao, W., Liu, Y., Zeng, Y., Liu, Q., & Li, Q. SAR Image Ship Target Detection Adversarial Attack and Defence Generalization Research. *Sensors*, 2023, vol. 23, no. 4. DOI: 10.3390/s23042266.

3. Asiyabi, R. M., Ghorbanian, A., Tameh, S. N., Amani, M., Jin, S. & Mohammadzadeh, A. Synthetic Aperture Radar (SAR) for Ocean: A Review. *IEEE Journal of Selected Topics in Applied Earth Observations and Remote Sensing*, 2023, vol. 16, pp. 9106–9138. DOI: 10.1109/JSTARS.2023.3310363.

4. Okada, Y., Nakamura, S., Iribe, K., Yokota, Y., Tsuji, M., Tsuchida, M., Hariu, K., Kankaku, Y., Suzuki, S., Osawa, Y., & Shimada, M. System design of wide swath, high resolution, full polarimietoric L-band SAR onboard ALOS-2. *2013 IEEE International Geoscience and Remote Sensing Symposium - IGARSS*, 2013, pp. 2408–2411. DOI: 10.1109/IGARSS.2013.6723305.

5. Datcu, M., Schwarz, G., Schmidt, K., & Reck, C. Quality Evaluation of Compressed Optical and SAR Images: JPEG vs. Wavelets. *Proc. of 1995 International Geoscience and Remote Sensing Symposium, IGARSS '95*, 1995, pp. 1687–1689. Available at: https://elib.dlr.de/23745/ (accessed 20 November 2025).

6. Kozhemiakin, R., Abramov, S., Lukin, V., Djurović, B., Djurović, I., & Simeunović, M. Strategies of SAR image lossy compression by JPEG2000 and SPIHT. *2017 6th Mediterranean Conference on Embedded Computing (MECO)*, 2017, pp. 1–6. DOI: 10.1109/MECO.2017.7977176.

7. Deng, J., & Huang, L. Synthetic Aperture Radar Image Compression Based on Low-Frequency Rejection and Quality Map Guidance. *Remote Sensing*, 2024, vol. 16, no. 5. DOI: 10.3390/rs16050891.

8. Rusyn, B., Lutsyk, O., Lysak, Y., Lukenyuk, A., & Pohreliuk, L. Lossless image compression in the remote sensing applications. *2016 IEEE First International Conference on Data Stream Mining & Processing (DSMP),* 2016, pp. 195–198. DOI: 10.1109/DSMP.2016.7583539.

9. Yin, D., Gu, Z., Zhang, Y., Gu, F., Nie, S., Feng, S., Ma, J., & Yuan, C. Speckle noise reduction in coherent imaging based on deep learning without clean data. *Optics and Lasers in Engineering*, 2020, vol. 133, article no. 106151. DOI: 10.1016/j.optlaseng.2020.106151.

10. Sun, Z., Leng, X., Zhang, M., Ren, H., & Ji, K. SAR Image Object Detection and Information Extraction: Methods and Applications. *Remote Sensing*, 2025, vol. 17, no. 12. DOI: 10.3390/rs17122098

11. Ko, J., & Lee, S. SAR Image Despeckling Using Continuous Attention Module. *IEEE Journal of Selected Topics in Applied Earth Observations and Remote Sensing*, 2022, vol. 15, pp. 3–19. DOI: 10.1109/JSTARS.2021.3132027.

12. Liu, Z., Wang, S., & Gu, Y. SAR Image Compression With Inherent Denoising Capability Through Knowledge Distillation. *IEEE Geoscience and Remote Sensing Letters*, 2024, vol. 21, pp. 1–5. DOI: 10.1109/LGRS.2024.3386758.

13. Ponomarenko, N. N., Lukin, V. V., Kozhemiakin, R. A., Egiazarian, K. O., & Chobanu, M. K. Lossy and visually lossless compression of single-look SAR images. *Telecommunications and Radio Engineering*, 2013, vol. 72, no. 8, pp. 711–729. DOI: 10.1615/TelecomRadEng.v72.i8.60.

14. Kryvenko, S., Lukin, V., & Vozel, B. Lossy Compression of Single-channel Noisy Images by Modern Coders. *Remote Sensing*, 2024, vol. 16, no. 12. DOI: 10.3390/rs16122093.

15. Odegard, J. E., Guo, H., Lang, M., Burrus, C. S., Jr., R. O. W., Novak, L. M., & Hiett, M. Wavelet-based SAR speckle reduction and image compression. *SPIE's 1995 Algorithms for Synthetic Aperture Radar Imagery II* 1995, vol. 2487, pp. 259–271. DOI: 10.1117/12.210843.

16. Yee, D., Soltaninejad, S., Hazarika, D., Mbuyi, G., Barnwal, R., & Basu, A. Medical image compression based on region of interest using better portable graphics (BPG). *2017 IEEE International Conference on Systems, Man, and Cybernetics (SMC)*, 2017, pp. 216–221. DOI: 10.1109/SMC.2017.8122605.

17. Lainema, J., Hannuksela, M., Malamal Vadakital, V., & Aksu, E. HEVC still image coding and high efficiency image file format. *2016 IEEE International Conference on Image Processing (ICIP)*, 2016, pp. 71–75. DOI: 10.1109/ICIP.2016.7532321.

18. Chen, Y., Mukherjee, D., Han, J., Grange, A., Xu, Y., Parker, S., Chen, C., Su, H., Joshi, U., Chiang, C.-H., Wang, Y., Wilkins, P., Bankoski, J., Trudeau, L., Egge, N., Valin, J.-M., Davies, T., Midtskogen, S., Norkin, A., & Liu, Z. An Overview of Coding Tools in AV1: the First Video Codec from the Alliance for Open Media. *APSIPA Transactions on Signal and Information Processing*, 2020, vol. 9. DOI: 10.1017/ATSIP.2020.2.

19. Bondzulic, B., Pavlović, B., Stojanovic, N., & Petrovic, V. Picture-wise just noticeable difference prediction model for JPEG image quality assessment.

ISSN 1814-4225 (print)
ISSN 2663-2012 (online)

Military Technical Courier, 2022, vol. 70, pp. 62–86. DOI: 10.5937/vojtehg70-34739

20. Lukin, V., Kryvenko, S., & Pavliuk, A. Visually lossless compression of multilook SAR images. *Aerospace Technic and Technology*, 2025, pp. 123–133. DOI: 10.32620/aktt.2025.4.12.

21. Jamil, S. Review of Image Quality Assessment Methods for Compressed Images. *Journal of Imaging*, 2024, vol. 10, no. 5. DOI: 10.3390/jimaging10050113.

22. Nafchi, H., Shahkolaei, A., Hedjam, R., & Cheriet, M. Mean Deviation Similarity Index: Efficient and Reliable Full-Reference Image Quality Evaluator. *IEEE Access*, 2016, vol. 4, pp. 5579–5590. DOI: 10.1109/ACCESS.2016.2604042.

23. Reisenhofer, R., Bosse, S., Kutyniok, G., & Wiegand, T. A Haar Wavelet-Based Perceptual Similarity Index for Image Quality Assessment. *Signal Processing Image Communication*, 2018, vol. 61, pp. 33–43. DOI: 10.1016/j.image.2017.11.001.

24. Al-Shaykh, O. K., & Mersereau, R. M. Lossy compression of noisy images. *IEEE Transactions on Image Processing*, 1998, vol. 7, no. 12, pp. 1641–1652. DOI: 10.1109/83.730376.

25. Rubel, O., Lukin, V., Rubel, A., & Egiazarian, K. Selection of Lee Filter Window Size Based on Despeckling Efficiency Prediction for Sentinel SAR Images. *Remote Sensing*, 2021, vol. 13, no. 10. DOI: 10.3390/rs13101887.

26. Lukin, V., Kolganova, O., & Kryvenko, S. Lossy Compression of Images Corrupted by Spatially Correlated Noise. *2016 13th International Conference on Modern Problems of Radio Engineering, Telecommunications and Computer Science (TCSET),* 2016, pp. 698-702. DOI: 10.1109/TCSET.2016.7452157.

27. *Sentinel-1*. Available at: https://sentinels.copernicus.eu/copernicus/sentinel-1 (accessed 20 November 2025).

28. Abdikan, S., Balik Sanli, F., Ustuner, M., & Calò, F. Land Cover Mapping Using SENTINEL-1 SAR Data. *ISPRS - International Archives of the Photogrammetry, Remote Sensing and Spatial Information Sciences*, 2016, pp. 757–761. DOI: 10.5194/isprs-archives-XLI-B7-757-2016.

29. Fan, D., Zhao, T., Jiang, X., García-García, A., Schmidt, T., Samaniego, L., Attinger, S., Wu, H., Jiang, Y., Shi, J., Fan, L., Tang, B.-H., Wagner, W., Dorigo, W., Gruber, A., Mattia, F., Balenzano, A., Brocca, L., Jagdhuber, T., & Peng, J. A Sentinel-1 SAR-based global 1-km resolution soil moisture data product: Algorithm and preliminary assessment. *Remote Sensing of Environment*, 2025, vol. 318, article no. 114579. DOI: 10.1016/j.rse.2024.114579

30. Di Martino, G., Poderico, M., Poggi, G., Riccio, D., & Verdoliva, L. SAR image simulation for the assessment of despeckling techniques. *2012 IEEE International Geoscience and Remote Sensing Symposium*, 2012, pp. 1797–1800. DOI: 10.1109/IGARSS.2012.6351163.

31. De Fioravante, P., Luti, T., Cavalli, A., Giuliani, C., Dichicco, P., Marchetti, M., Chirici, G., Congedo, L., & Munafò, M. Multispectral Sentinel-2 and SAR Sentinel-1 Integration for Automatic Land Cover Classification. *Land*, 2021 vol. 10, no. 6, article no. 611. DOI: 10.3390/land10060611.

32. Li, F., Ieremeiev, O., Lukin, V., & Egiazarian, K. BPG-Based Lossy Compression of Three-Channel Remote Sensing Images with Visual Quality Control. *Remote Sensing*, 2024, vol. 16, no. 15, article no. 2740. DOI: 10.3390/rs16152740.

33. Zemliachenko, A. N., Lukin, V. V., Ponomarenko, N. N., Egiazarian, K. O., & Astola, J. Still image/video frame lossy compression providing a desired visual quality. *Multidimensional Systems and Signal Processing*, 2016, vol. 27, no. 3, pp. 697–718. DOI: 10.1007/s11045-015-0333-8.

Отримано 11.08.2025, отримано у доопрацьованому вигляді 20.09.2025
Дата ухвалення 17.11.2025, дата публікації 08.12.2025

СТИСНЕННЯ БАГАТОВИГЛЯДОВИХ РСА-ЗОБРАЖЕНЬ З ВТРАТАМИ В ОКОЛІ ОПТИМАЛЬНОЇ РОБОЧОЇ ТОЧКИ КОДЕРОМ BPG

В. В. Лукін, В. С. Ребров, А. Д. Павлюк

Предметом статті є стиснення з втратами багатопоглядових зображень, що отримані радіолокатором із синтезованою апертурою (РСА) та спотворені мультиплікативним просторово корельованим спекл-шумом, з акцентом на роботу поблизу потенційної оптимальної робочої точки (ОРТ). **Метою** статті є аналіз існування та властивостей ОРТ для РСА-зображень, стиснених за допомогою кодера. Better Portable Graphics (BPG), та розробка практичного методу досягнення стиснення поблизу цієї точки. **Завдання**, що потребують вирішення: перевірити існування ОРТ для змодельованих РСА-зображень, подібних до Sentinel-1, згідно з традиційними метриками пікового співвідношення сигнал/шум (PSNR) та візуальної якості (PSNR-HVS-M); дослідити взаємозв'язок між параметром керування стисненням (Q) та результуючою якістю зображення та коефіцієнтом стиснення (CR); розробити практичну ітераційну процедуру для визначення значення параметра Q, що відповідає ОРТ, без необхідності доступу до опорного зображення без шуму. Використані **методи**:

моделювання РСА-зображень з відносною дисперсією спеклу, що дорівнює 0,05, з використанням даних Sentinel-2 без шуму як еталону; стиснення з втратами за допомогою BPG-кодера з параметром Q, що змінюється від 1 до 51; кількісна оцінка за допомогою метрик PSNR та PSNR-HVS-M; розрахунок коефіцієнта стиснення; аналіз кривих швидкість/спотворення для різних пар зображень; статистична оцінка еквівалентної дисперсії шуму для прогнозування PSNRn. Отримані наступні **результати:** продемонстровано, що для BPG-кодеру існує ОРТ під час стиснення багатопоглядових РСА-зображень, що підтверджено як PSNR, так і PSNR-HVS-M метриками. ОРТ забезпечує значення PSNR та PSNR-HVS-M на кілька дБ вищі, ніж у нестиснутого зображення з шумом, досягаючи при цьому дуже високих коефіцієнтів стиснення (CR > 180). ОРТ було виявлено при високих значеннях Q = 48 - 49, де кодер агресивно пригнічує шум, але також вносить спотворення вмісту. Ключовим практичним результатом є запропонований метод визначення Q в ОРТ. **Висновки**. Наукова новизна отриманих результатів полягає в наступному: вперше існування ОРТ продемонстровано для BPG-кодера, застосованого до багатопоглядових РСА-зображень з реалістичними властивостями спеклу, враховуючи не лише стандартний PSNR, але й метрику візуальної якості PSNR-HVS-M, хоча для останньої ОРТ менш виражений; розроблено метод практичного досягнення ОРТ, який працює без необхідності використання оригінального (істинного) зображення, спираючись на оцінку потужності спекл-шуму з доступних зашумлених даних, що робить його застосовним у реальних сценаріях обробки та передачі РСА-зображень.

Ключові слова: радар з синтезованою апертурою, стиснення з втратами, зображення зі спеклом, оптимальна робоча точка.

Лукін Володимир Васильович – д-р техн. наук, проф., зав. каф. інформаційно-комунікаційних технологій ім. О. О. Зеленського, Національний аерокосмічний університет «Харківський авіаційний інститут», Харків, Україна.

Ребров Володимир Сергійович – асп. каф. інформаційно-комунікаційних технологій ім. О.О. Зеленського, Національний аерокосмічний університет «Харківський авіаційний інститут», Харків, Україна.

Павлюк Андрій Дмитрович – асист. каф. мат. моделювання та аналізу даних, Національний технічний університет України «Київський політехнічний інститут імені Ігоря Сікорського», Київ, Україна.

Vladimir Lukin – Doctor of Technical Sciences, Professor, Head of the Department of Information and Communication Technologies named after O. O. Zelensky, National Aerospace University "Kharkiv Aviation Institute", Kharkiv, Ukraine,
e-mail: v.lukin@khai.edu, ORCID: 0000-0002-1443-9685.

Volodymyr Rebrov –PhD Student of the Department of Information and Communication Technologies named after O. O. Zelensky, National Aerospace University "Kharkiv Aviation Institute", Kharkiv, Ukraine,
e-mail: r.volodymyr@khai.edu, ORCID: 0000-0002-6442-3155.

Andrii Pavliuk – Assistant at the Department of Mathematical Modeling and Data Analysis, National Technical University of Ukraine «Igor Sikorsky Kyiv Polytechnic Institute», Kyiv, Ukraine,
e-mail: andpa-ipt21@lll.kpi.ua, ORCID: 0009-0002-7283-6360.